Electronic Supplementary Material (ESI) for Materials Horizons.

Supplementary Information

Borohydride and Halide Dual-Substituted Lithium Argyrodites

Ji Hoon Han, Do Kyung Kim, Young Joo Lee, Young-Su Lee, Kyung-Woo Yi, Young Whan Cho**

1. Experimental section

1.1 Materials and synthesis

Materials Preparation: Li_3PS_4+x$LiBH_4$+y$LiCl$+z$LiBr$+kLiI solid electrolytes were prepared using a two-step ball-milling method. Lithium sulfide (Li_2S, Alfa Aesar, 200 mesh, 99.9%), phosphorus pentasulfide (P_2S_5, Sigma Aldrich, 99%), lithium chloride/lithium bromide/lithium iodide (LiCl/LiBr/LiI, Sigma Aldrich, 99%), and lithium borohydride ($LiBH_4$, Acros Organics, 95%) powders were used as starting materials. First, using a planetary mill (Retsch PM200), the Li_2S and P_2S_5 powders were mixed in a 3:1 molar ratio and placed into a lab-made 120 cm^3 zirconia bowl with 45 zirconia balls (10 mm in diameter) and milled at 650 rpm for 2 h. As explained in the manuscript, $LiBH_4$ causes an intense and spontaneous reaction with P_2S_5 during milling, which could be dangerous. Therefore, Li_2S and P_2S_5 were milled in the first step to form β-Li_3PS_4, and then $LiBH_4$ and LiX (X = Cl, Br, I) were added in the second step. We added 2.5 wt% toluene as a process control agent to prevent excessive sticking of powder around the bottom corner of the bowl during milling. The ball milling was paused every 5 min to avoid increasing the sample temperature too much. In the second step, $LiBH_4$ and LiCl powders were added and further ball-milled for 3 h. The samples were handled in an Ar-filled glovebox (O_2 and H_2O levels < 0.1 ppm). Li_6PS_5Cl was supplied by POSCO JK SOLID SOLUTION. A $LiNbO_3$-coated $LiNi_{0.8}Co_{0.1}Mn_{0.1}O_2$ and a conducting agent (Super P) was supplied by Hyundai Motor Group. Li_7PS_6 was synthesized following the methodology outlined in the reference.[1]

1.2 Characterization

X-ray powder diffraction (XRD) analysis: XRD analysis (D8 ADVANCE, Bruker AXS, with Cu Kα radiation (λ = 1.540598 Å)) was performed over the 2θ range of 10°–90° with a step size of 0.028° to analyze the crystal structure. Because of the air sensitivity, all the samples were sealed using a 7.5-μm-thick polyimide film with a lab-made sample holder in the glove box.

Rietveld refinement analysis: Rietveld refinement was performed using TOPAS v.5 software (Bruker AXS) over the 2θ range of 10°–90°.[2] Because the limited quality of the XRD data did not allow us to refine the position of H in BH_4^-, the B–H bond length was fixed to 1.1 Å, the usual bond length of B–H obtained from XRD.[3] Within the symmetry of F–43m, there are two possible orientations of BH_4^-, and we assumed an equal occupancy for the two orientations. The T5 site for 48h, as shown in **Table 1** in manuscript, and the corresponding position presented in the **Supplementary Information** were reported by the same research group alongside the neutron diffraction data. However, the former achieved improved accuracy by incorporating the value of "R_{mean}".[4] R_{mean} is calculated as the average distance between the three distinct Li sites and their respective central anion at the 4d site. Consequently, to minimize the error associated with the position of Li, the 48h Li position in **Table 1**, which has a lower R_{wp} value, is presented as a representative. Although minor variations exist, the observed trend of increasing BH_4^- occupancy with increasing x remained consistent.

We assumed that all 0.5 Cl^- occupies 4a and 4d sites evenly. Generally, when more halide anions enter into the argyrodite structure, the degree of S^{2-}/Cl^- disorder at the 4a and 4d sites increases, being closer to a uniform distribution.[5] For $Li_{7-x}PS_{6-x}Cl_x$ ($1.5 \leq x \leq 1.75$) and $Li_{5.3}PS_{4.3}ClBr_{0.7}$, it was reported that Cl^- and Br^- are almost uniformly distributed over the 4a and 4d sites.[6, 7] Therefore, the assumption of uniform distribution of Cl^- seems reasonable. Another important parameter is the amount of Cl^- anion in the argyrodite structure. When x in Li_3PS_4+x$LiBH_4$+0.5LiCl is lower than 2.5, free LiCl was not observed in either the XRD or solid-state NMR data. Because the LiCl structure is not easily destroyed by ball milling, it would have been detected by XRD if it had existed. Therefore, we expect that 0.5 mol of LiCl was incorporated into the argyrodite structure. When x is 2.5, a small amount of residual LiCl was observed in the XRD and solid-state NMR data. However, the first main peak of LiCl overlapped with the argyrodite phase, and the intensities of other peaks were too small to quantify; in addition, we assume that the amount of free LiCl is very minor and that the majority of 0.5 LiCl appears in the argyrodite structure. Therefore, the occupancy of Cl^- was set to 0.25 both at the 4a and 4d sites, and the sum of the occupancies of BH_4^- and S^{2-} was set to 0.75. For the background, since XRD was measured with a 7.5-micron kapton film, the background peak of the kapton film was excluded during the Rietveld refinement (**Fig. S12**).

Differential scanning calorimetry (DSC) measurement: DSC analysis was performed using a Netzsch Polyma 214 to evaluate the thermal properties. About 2 mg of the sample was sealed in an Al_2O_3 crucible, and a hole was drilled immediately before measurement to minimize contact with the atmosphere. Dry air flowed with a rate of 20 cm^3 min^{-1}, and the temperature was increased to 200 °C at 10 K min^{-1}.

Solid-state nuclear magnetic resonance (NMR) spectroscopy: Solid-state NMR experiments were performed on a Bruker Neo 600 spectrometer equipped with a 3.2-mm triple-resonance magic angle spinning (MAS) probe. ^{7}Li MAS NMR spectra were obtained at an operating frequency of 233.17 MHz with 45° pulse lengths of 3.4 μs and a MAS frequency of 22 kHz. ^{31}P MAS NMR spectra were obtained at an operating frequency of 242.87 MHz with 90° pulse lengths of 3.75 μs and a MAS frequency of 22 kHz. ^{11}B MAS NMR spectra were obtained at an operating frequency of 192.49 MHz with 45° pulse lengths of 2.15 μs and a MAS frequency of 22 kHz. A TRIP pulse sequence was used to suppress the ^{11}B background signal. All spectra were represented as chemical shifts (δ) and referenced to 1M LiCl (aq.) at 0 ppm, H_3PO_4 (aq.) at 0 ppm and $B(OH)_3$ at 0 ppm, for ^{7}Li, ^{31}P and ^{11}B NMR, respectively.

Electrochemical impedance spectroscopy (EIS): With an SS (SUS440C)/solid electrolyte/SS cell, the ionic conductivity was measured using EIS (IviumStat.h, Ivium Technologies). A 120-mg sample was placed into a 6-mm diameter mold made of zirconia, cold-pressed at 566 MPa, and then, measurements were performed at 188 MPa and 25 °C. The frequency range was from 1 MHz to 100 Hz at an amplitude of 100 mV.

Cyclic voltammetry (CV) measurement: CV was conducted to evaluate the electrochemical stability of the solid electrolyte. First, the appropriate amount of the electrolyte was pressed at 68 MPa into a polyether ketone (PEEK) mold to form a pellet. The working electrode was a SS (SUS440C) plunger, and the counter/reference electrode was 9-mm diameter Li metal sheet affixed to the top side (Li/SE/SS). The CV curves were obtained using a potentiostat (VMP3, BioLogic) between −0.1 and 5.0 V at 30 °C and a scan rate of 1 mV s^{-1}, repeated 3 times.

Lithium symmetric cell and critical current density measurement: A Li symmetric cell was assembled to test the lithium deposition and dissolution, and 1,000 cycles were performed for 1 h each (WBCS3000L, WonATech). The as-synthesized electrolyte powder was placed into a 10-mm-diameter mold and cold-pressed at 312 MPa. Then 9-mm-diameter Li-metal sheets were placed on both sides of the mold (Li/SE/Li). Finally, the mold was assembled under a constant torque of 7 N m and measured at 30 °C. The current densities applied were 0.1 and 1 mA cm^{-2}. The critical current density was measured after assembling in the same method as the Li symmetric cell. The time for each charge and discharge is 1 h, and step size for the current increase is 0.1 mA cm^{-2} for the Time-constant mode. For the Capacity-constant mode, the initial current density was 0.5 mA cm^{-2}, and increased by 0.25 mA cm^{-2} after each cycle. The half-cycle capacity is 2 mAh cm^{-2}.

Fabrication and Characterization of ASSB Cells: Metal sheets consisting of Li foil served as the anode for the cell test. The cathode composites were composed of $LiNbO_3$-coated $LiNi_{0.8}Co_{0.1}Mn_{0.1}O_2$ (70 wt%), a conducting agent (Super P, 5 wt%), and the solid electrolyte (25 wt%). For the cell assembly, the synthesized solid-electrolyte powders (150 mg) were placed in a PEEK mold with a 10-mm diameter and then pressed at 312 MPa. The cathode composites (9 mg) were added on the top of the solid-electrolyte pellet with aluminum foil (10-mm diameter, current collector) and pressed at 368 MPa. The other side was a Li-foil anode (9-mm diameter, 2-mm thickness) with copper foil (10-mm diameter, current collector). The cells were assembled in the glovebox and galvanostatically tested at various current densities at 30 °C under normal atmospheric conditions with sealing. Based on well-known theoretical specific capacity of NCM811 (~200 mAh g^{-1}), we calculated the practical capacity to be 200 mAh g^{-1}. And 1 C was calculated based on the total mass of the cathode mixture (70 wt% of 9 mg): 1 C = 200 mAh $g^{-1} \times 0.009$ g $\times$ 70 wt% = 1.26 mA. A battery cycler (WBCS3000L, WonATech) was used to determine the ASSB rate properties and for cycling testing and had a voltage cut off range between 2.7 and 4.3 V (as compared to Li^+/Li). The electrochemical performance was characterized at 0.05, 0.1, 0.2, 0.5, 1.0, and 2.0 C. The electrode thickness is 1.6 mm at the anode and 55 μm at the cathode (**Fig. S13**). For the cell using Li–In foil as the anode, a voltage cut off range between 2.1 and 3.7 V (as compared to Li^+/Li–In) was adopted.

2. Supplemental Figures and Tables

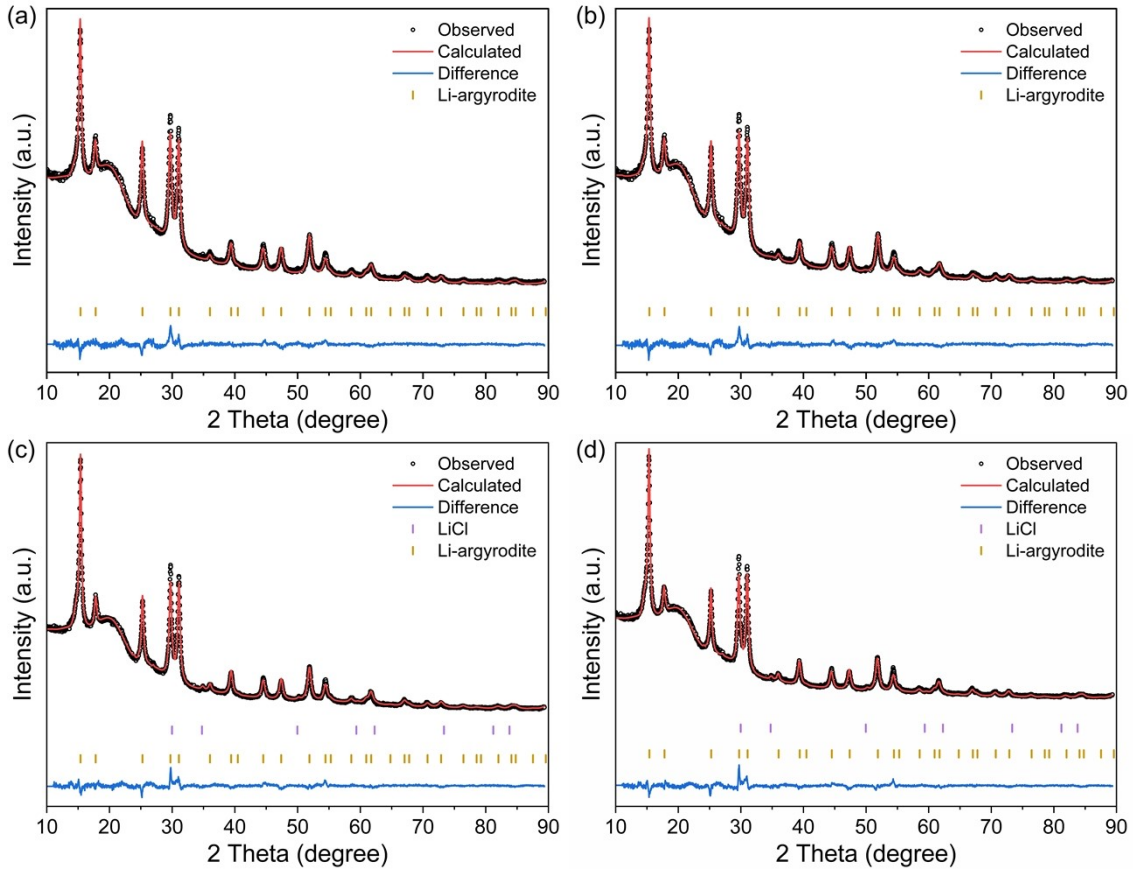

Fig. S1. Rietveld refinement profiles for Li_3PS_4+x$LiBH_4$+0.5LiCl (1.5 ≤ x ≤ 2.5) ((a) x = 1.5, (b) x = 1.75, (c) x = 2.25, (d) x = 2.5). See **Table S8-11** for detailed data.

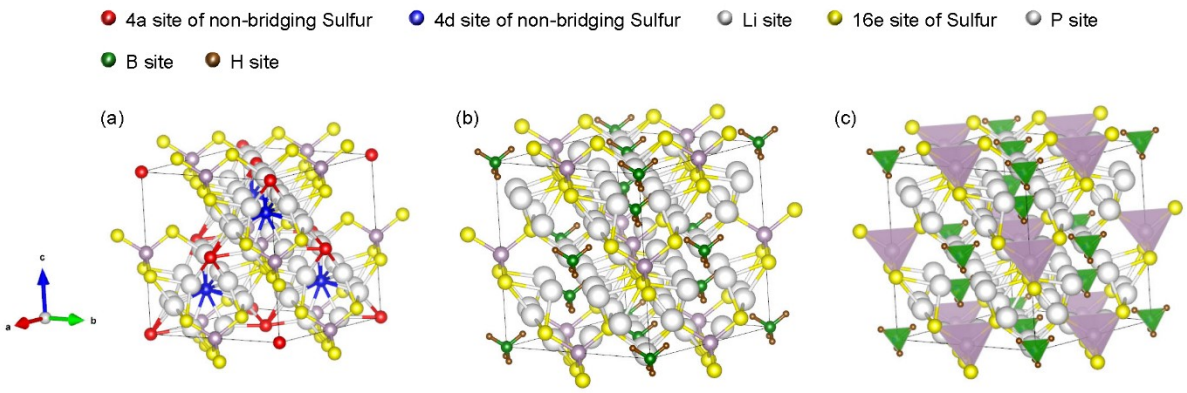

Fig. S2. (a) General structure of Li argyrodite; (b) structure of BH_4-substituted argyrodite; (c) BH_4-substituted argyrodite with illustrated PS_4 and BH_4 tetrahedral, respectively. PS_4 is represented as violet and BH_4 is represented as green. For the convenience of visualization, the directionality of H in BH_4 was not taken into consideration. The structure was visualized by VESTA 3 software.[8]

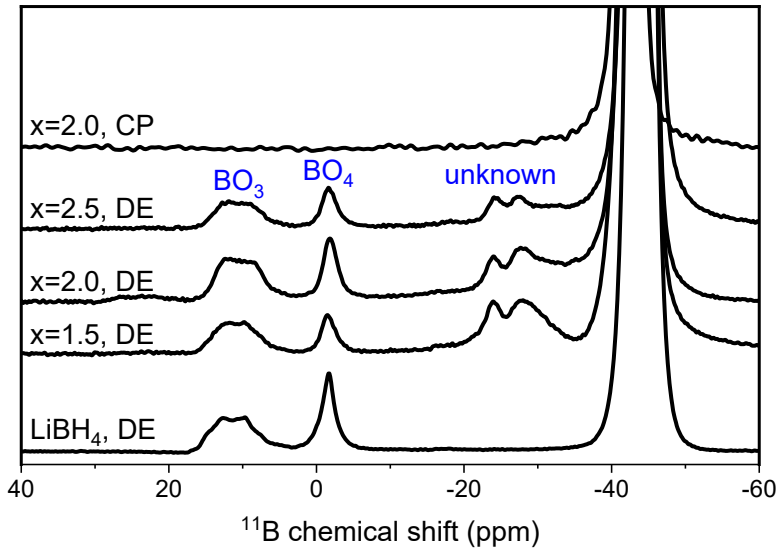

Fig. S3. Expansion of ^{11}B MAS with direct excitation (DE) and $^{11}B\{^{1}H\}$ cross polarization (CP) MAS NMR spectra of Li_3PS_4+x$LiBH_4$+0.5LiCl with x = 1.5, 2.0, and 2.5 and $LiBH_4$. Signals resulting from borate (BO_3, BO_4) and unknown impurities are denoted in the spectra. These impurity signals are not seen in the CP MAS NMR spectra, verifying that the chemical structures of the impurity phases are boron species with no associated protons. To suppress background signals, a TRIP pulse sequence was used for the ^{11}B DE MAS NMR experiments.

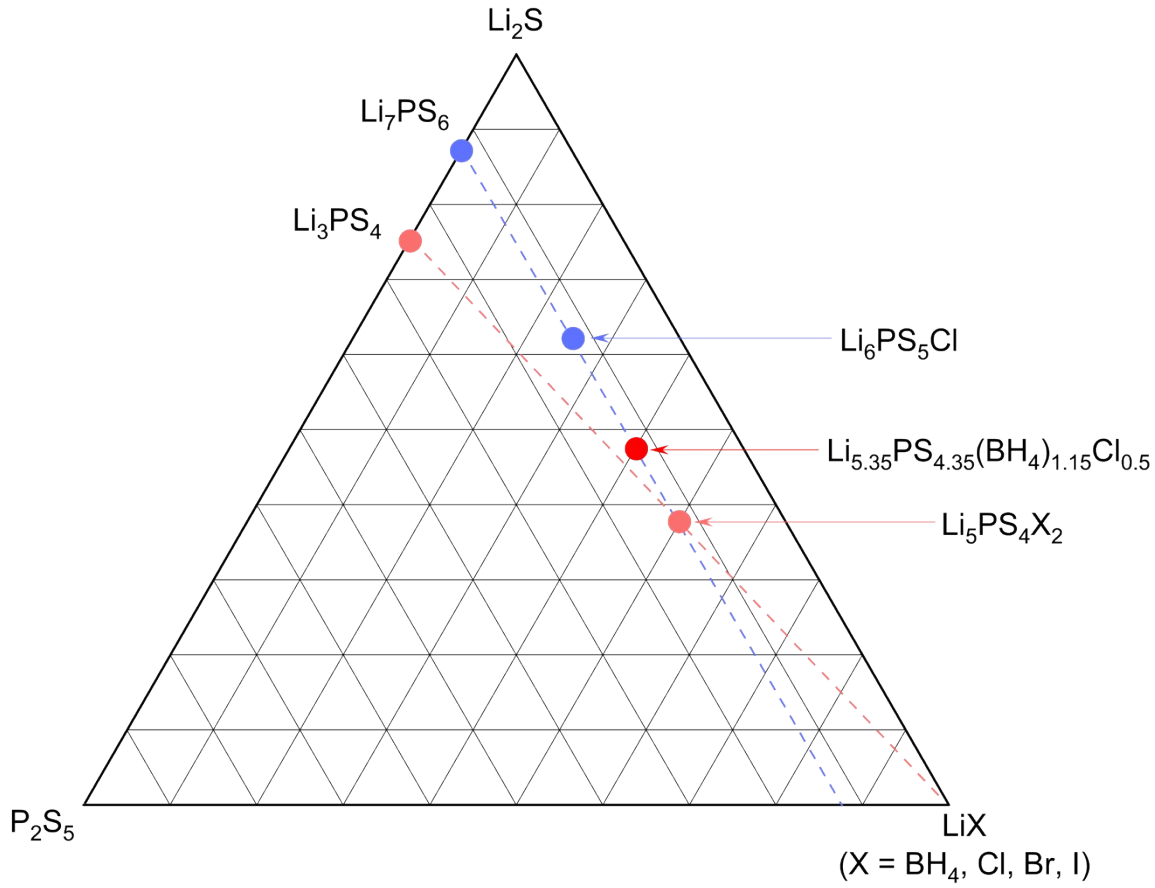

Fig. S4. Ternary phase diagram of Li_2S–P_2S_5–LiX. The chemical composition of $Li_{5.35}PS_{4.35}(BH_4)_{1.15}Cl_{0.5}$ deviates from the red dashed line connecting Li_3PS_4 and LiX. It instead falls on the line connecting $Li_5PS_4X_2$ and $LiPS_5Cl$. Therefore, an extra phase must exist in addition to the argyrodite-type phase after synthesis.

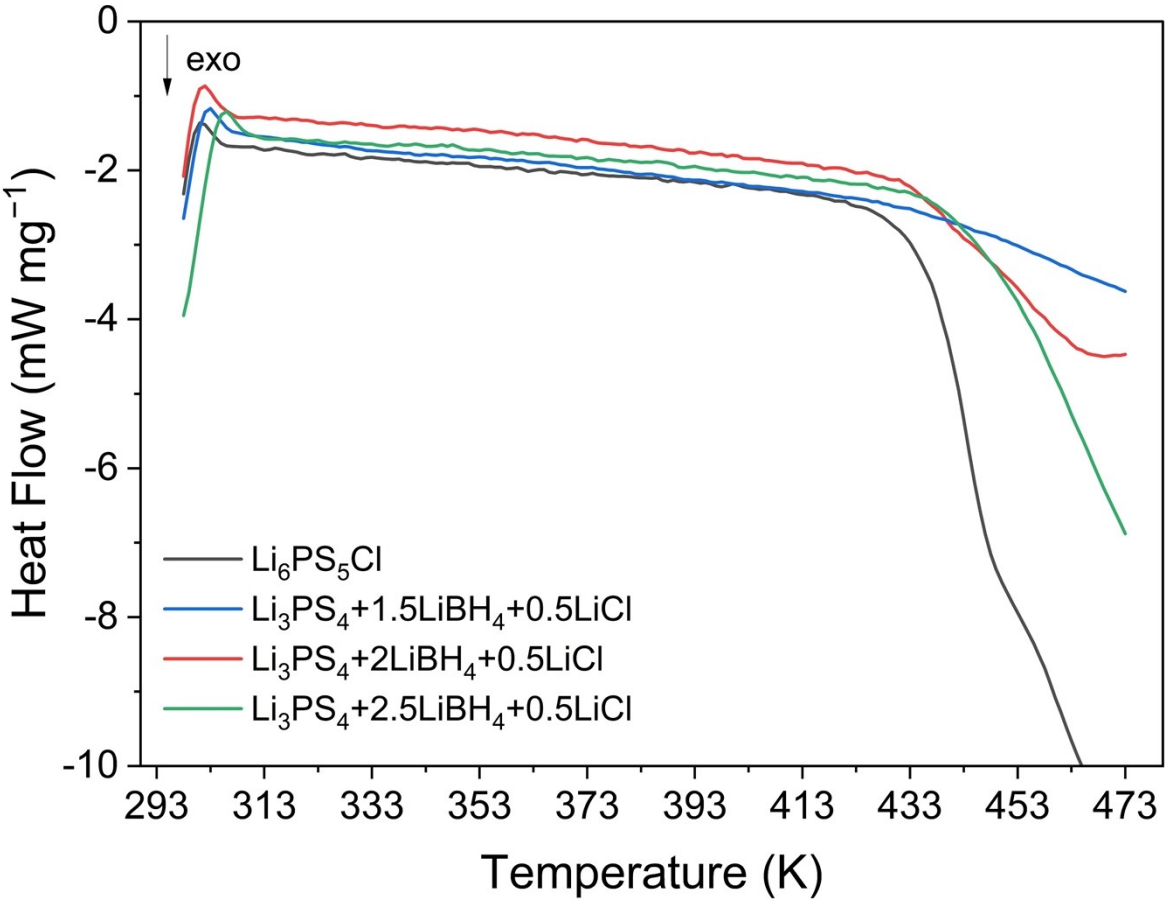

Fig. S5. DSC curve of commercial Li_6PS_5Cl, Li_3PS_4+x$LiBH_4$+0.5LiCl (x = 1.5, 2, 2.5). Dry air flowed with a rate of 20 cm^3 min^{-1}. The temperature was raised up to 200 °C at a rate of 10 K min^{-1}.

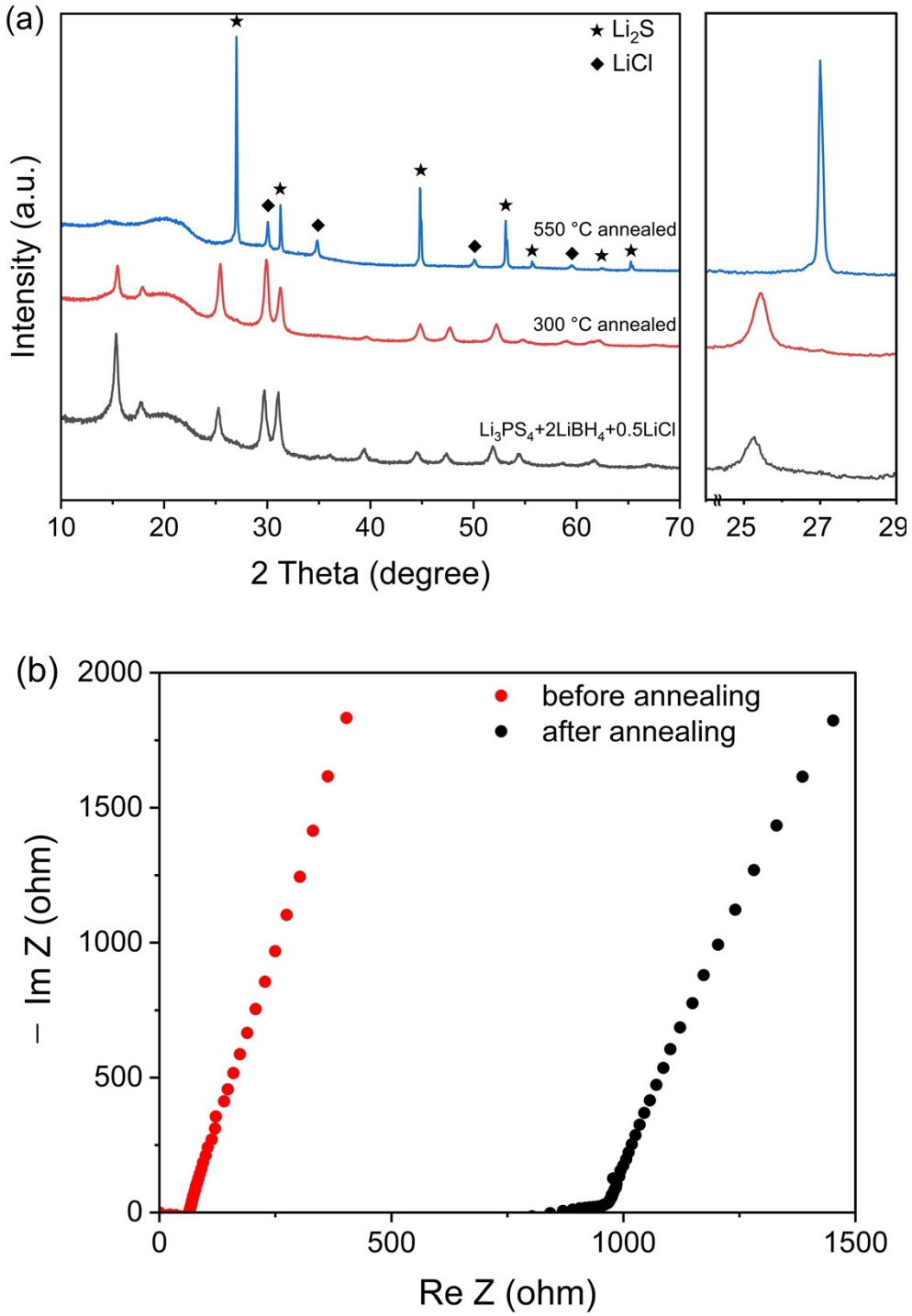

Fig. S6. (a) XRD data of Li_3PS_4+2$LiBH_4$+0.5LiCl and the samples annealed at 300 °C and 550 °C. The main peaks of the sample annealed at 300 °C shifted to higher angles, indicating the increased S^{2-} occupancy replacing the decomposed BH_4^-. (b) EIS data of Li_3PS_4+2$LiBH_4$+0.5LiCl and the samples annealed at 300 °C. The total resistance increased by

about 15 times, and the conductivity was measured to be 1.2 mS cm^{-1} after annealed at 300 °C.

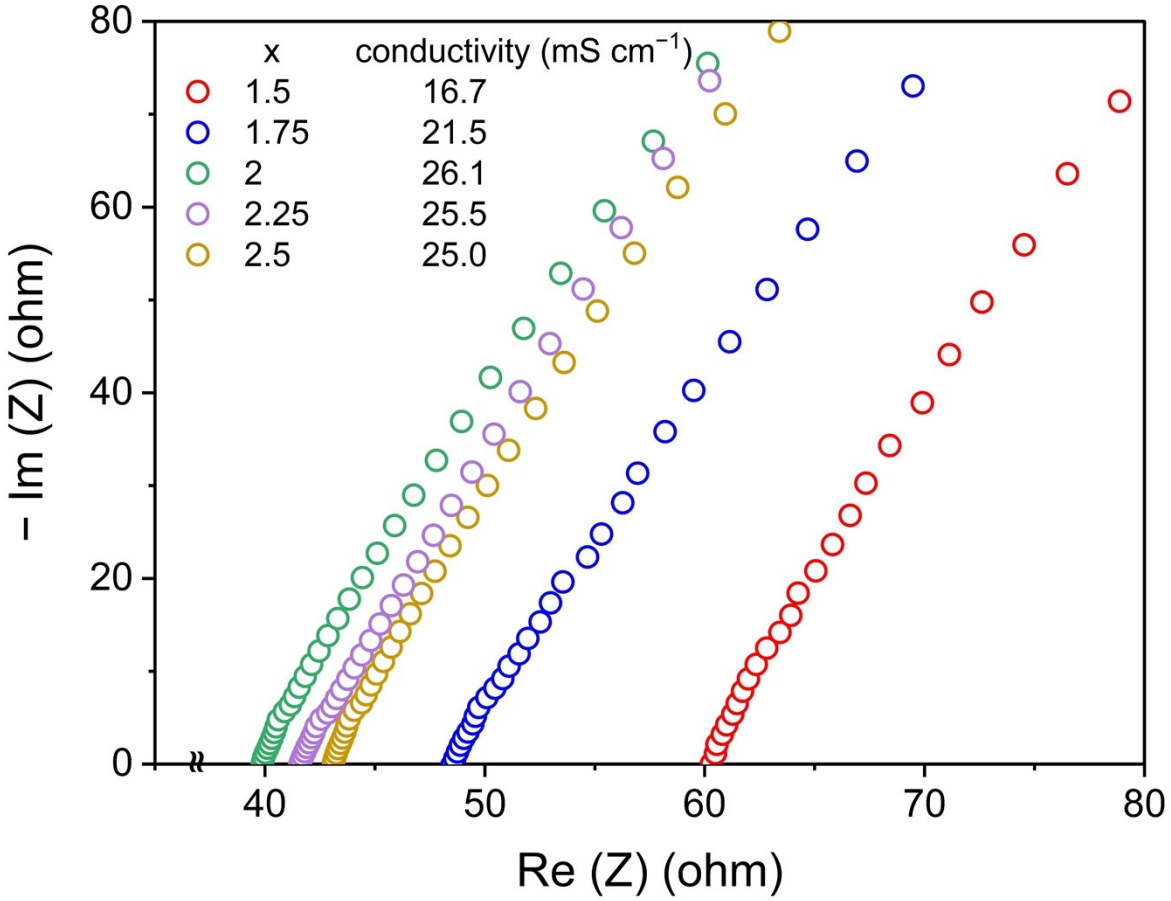

Fig. S7. Ionic conductivity and total resistance after warm pressing at 120 °C for 2 h. The data were measured at 25 °C, 188 MPa.

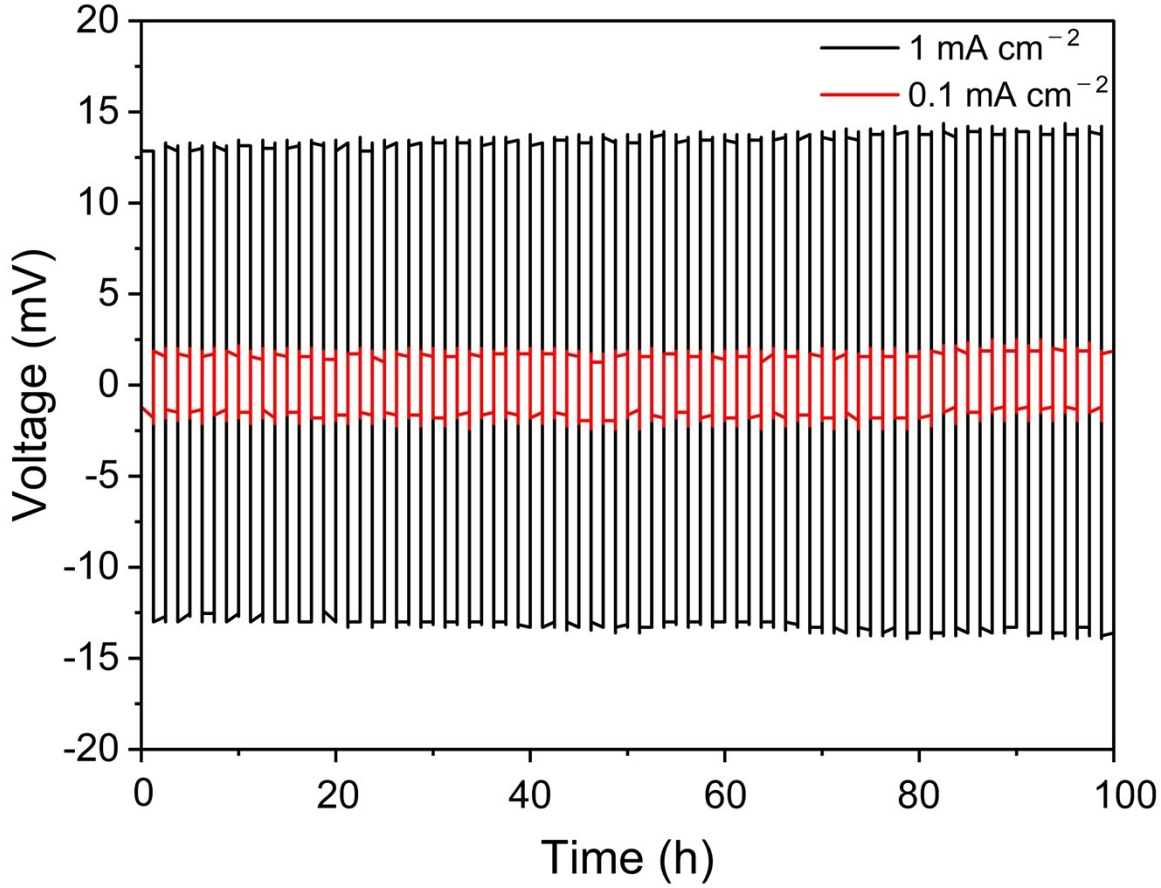

Fig. S8. Voltage profiles of the Li metal/Solid electrolyte/Li metal symmetric cells at 0.1 mA cm^{-2} and 1 mA cm^{-2}. At lower current density of 0.1 mA cm^{-2}, the overpotential for deposition and dissolution was less (2.5 mV) than at higher current density of 1 mA cm^{-2} (~12.5 mV). The overpotential did not change significantly up to 50 cycles, and no other side reactions were observed.

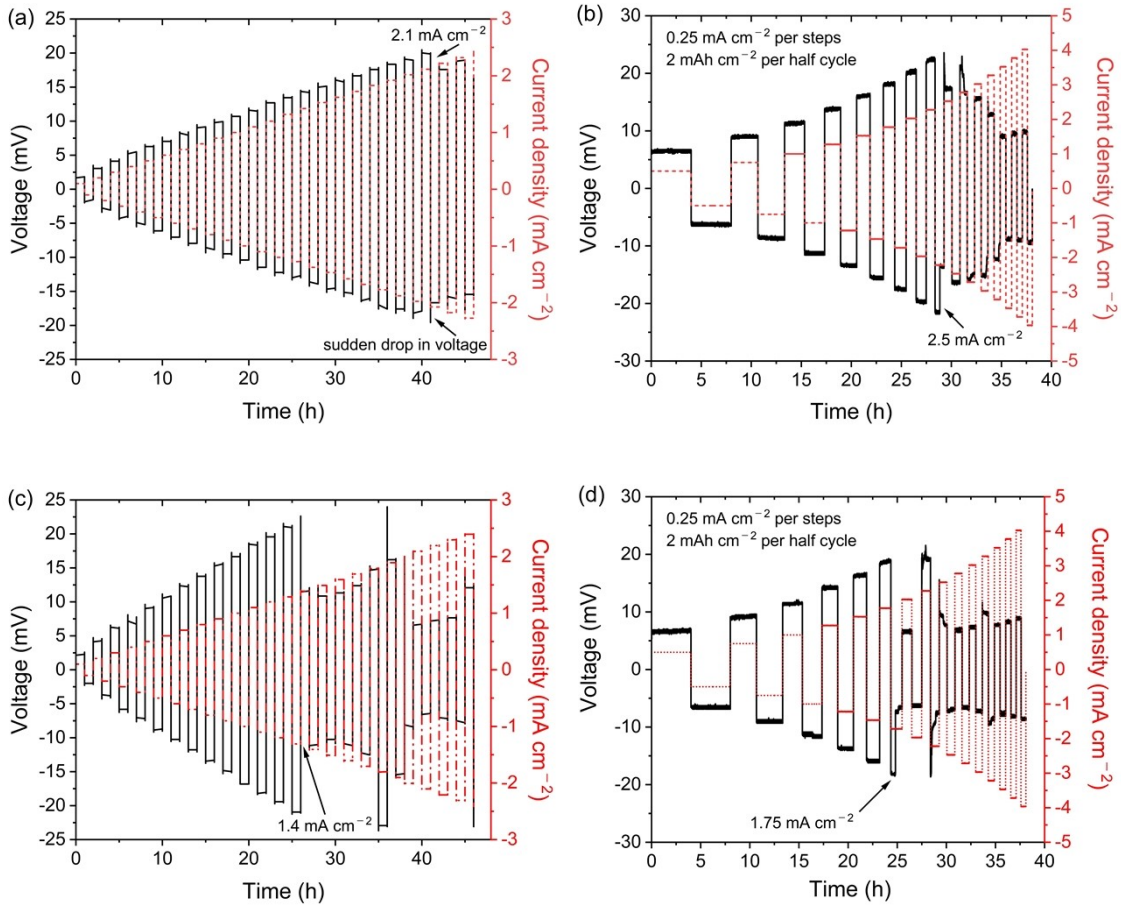

Fig. S9. The critical current density profile using the time-constant mode and the capacity constant mode, utilizing cold-pressed SE, was obtained at a temperature of 30 °C (Li metal/solid electrolyte/Li metal). The profile (a) and (b) were measured with $Li_{5.35}PS_{4.35}(BH_4)_{1.15}Cl_{0.5}$, and (c) and (d) with $Li_{5.59}PS_{4.59}(BH_4)_{1.41}$. The duration time for each charge and discharge was 1 h. The step size for the current density increase was 0.1 mA cm^{-2} for the time-constant mode. The half-cycle capacity was 2 mAh cm^{-2} and the current density was increased by 0.25 mA cm^{-2} after each cycle for the capacity-constant mode. By dual-substitution of BH_4 and Cl, the ionic conductivity increased, and it can be seen that the critical current density increased compared to the electrolyte in which only BH_4 was substituted.

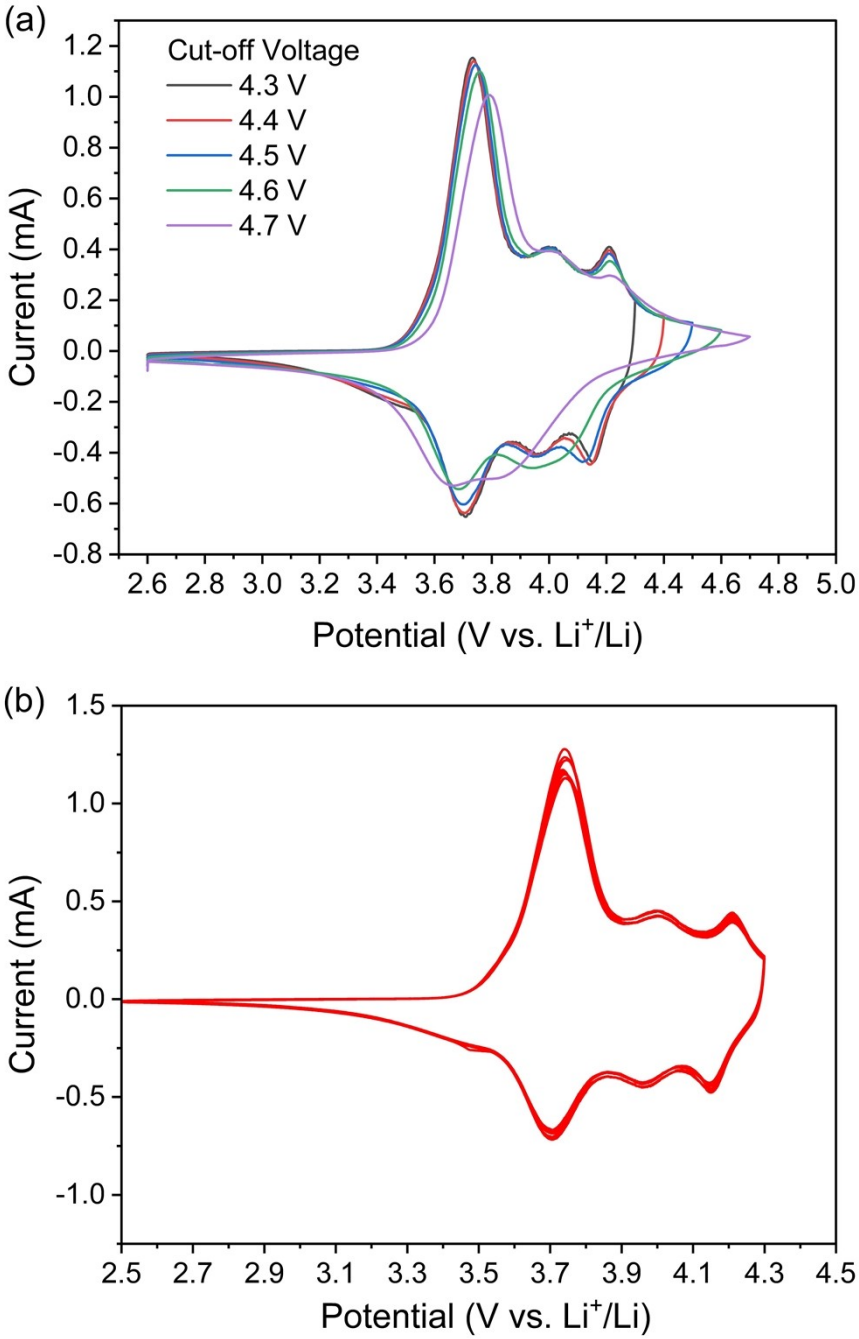

Fig. S10. (a) CV curves of Li/solid electrolyte ($Li_{5.35}PS_{4.35}(BH_4)_{1.15}Cl_{0.5}$)/cathode mixture (NCM 811, SE, Super C). The cut-off voltage increased from 4.3 V to 4.7 V, and the scanning speed was 0.1 mV s^{-1}. The overall measurements were conducted from 2.6 V to 4.7 V. (b) 10 cycles of CV curves for the Li/solid electrolyte ($Li_{5.35}PS_{4.35}(BH_4)_{1.15}Cl_{0.5}$)/cathode mixture (NCM 811, SE, Super C). The cut-off voltage was set to 4.3 V, and the scanning speed was maintained at 0.1 mV s^{-1}.

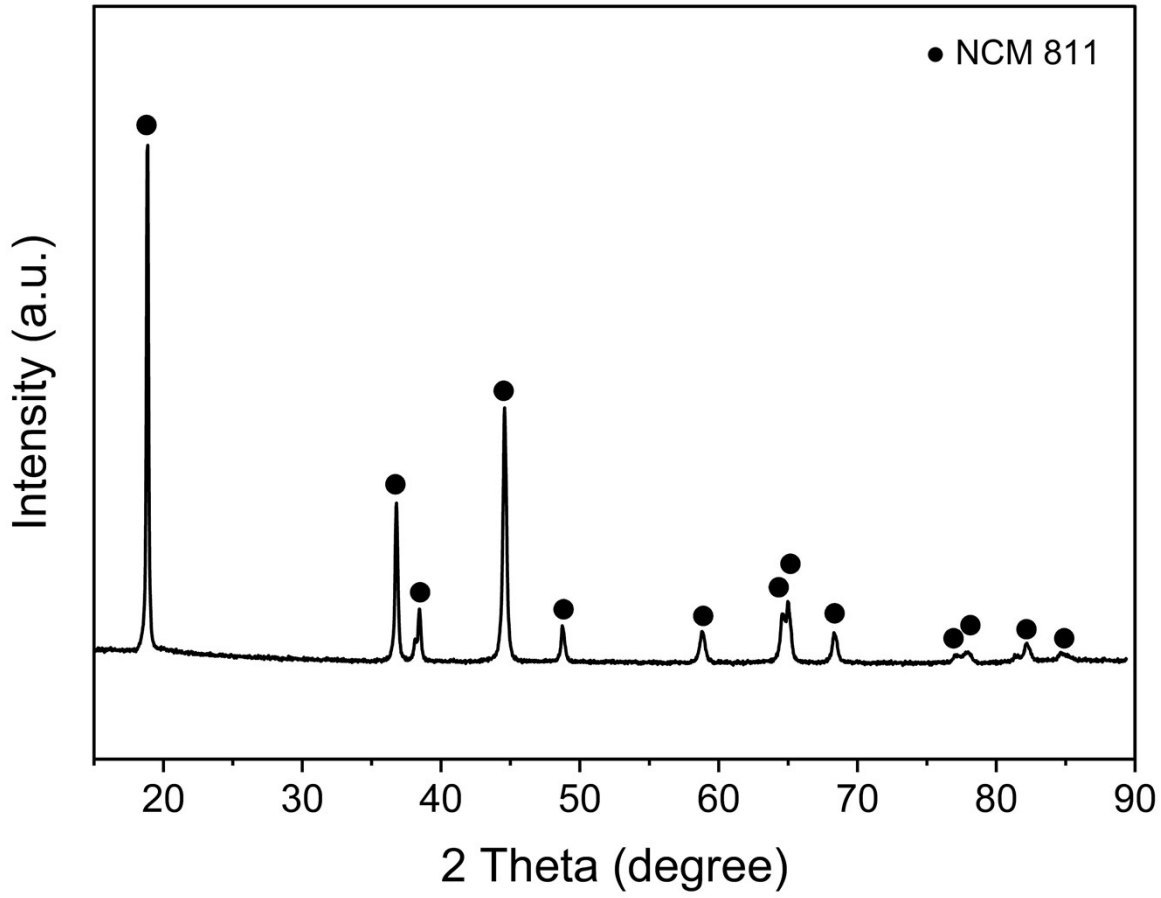

Fig. S11. XRD data of $LiNbO_3$-coated NCM 811 is presented, with NCM 811 being chosen for its relatively high energy density (~200 mAh g^{-1}).

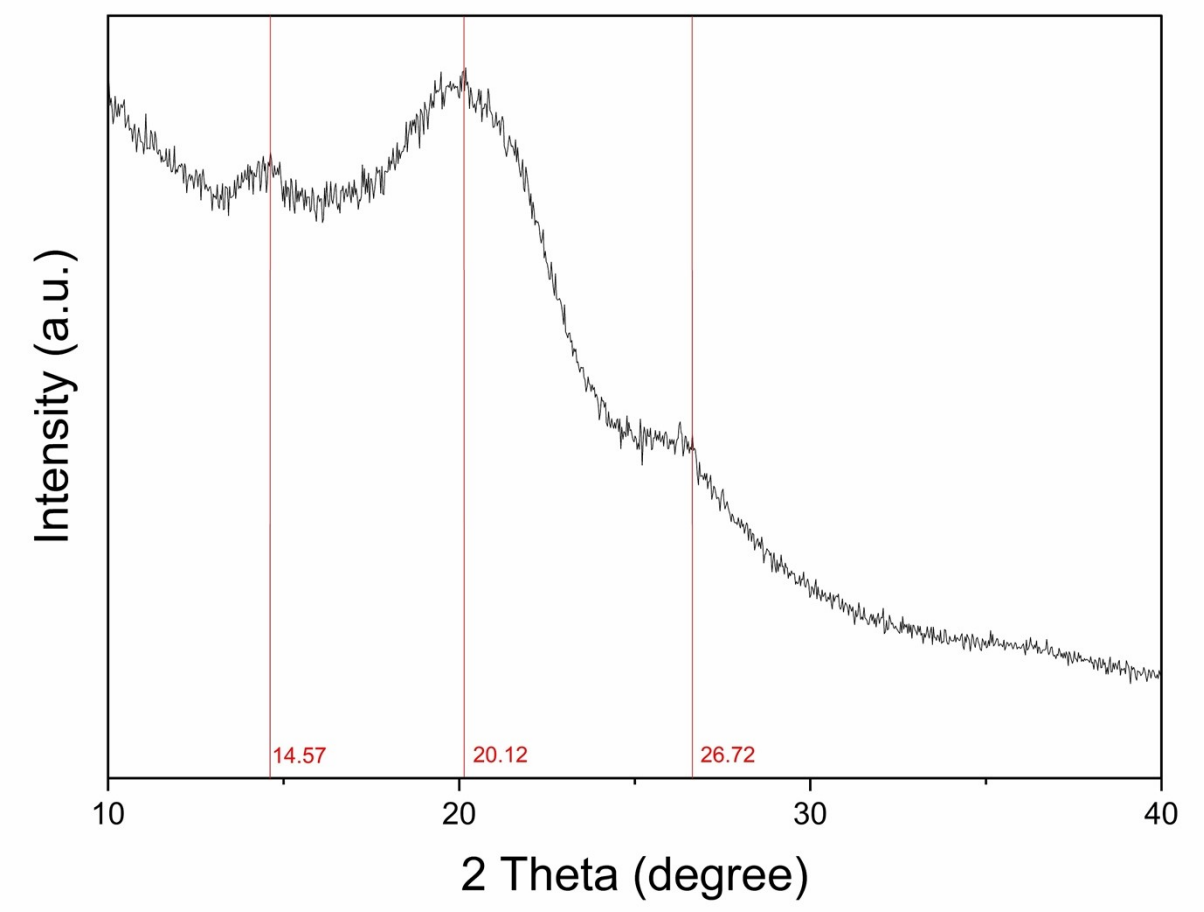

Fig. S12. 7.5-micron polyimide film's XRD data used with XRD measurements. This background peak was excluded while the Rietveld refinement (at 2θ = 14.57, 20.12, and 26.72).

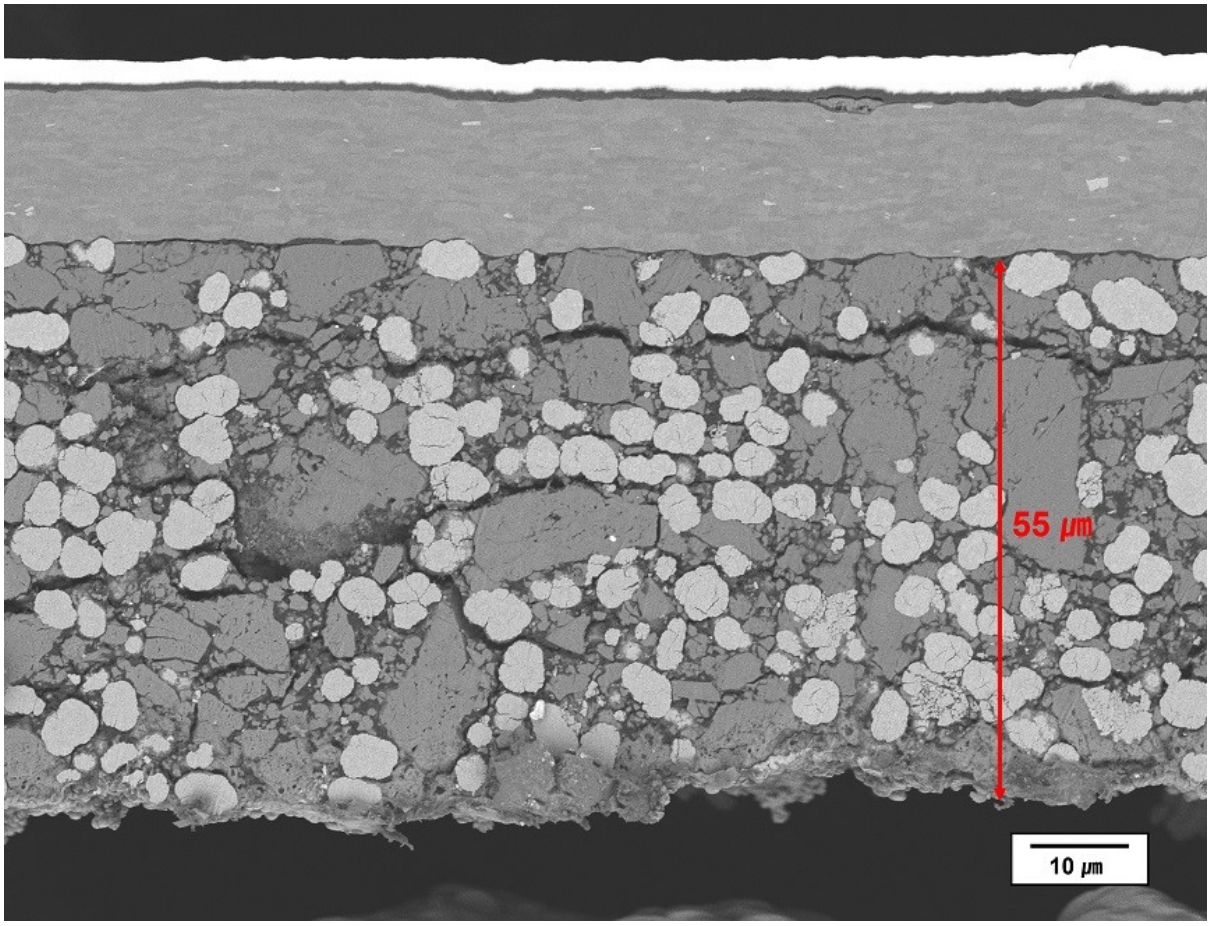

Fig. S13. Cross section image of the cathode. It can be seen that the thickness of the cathode is about 55 µm.

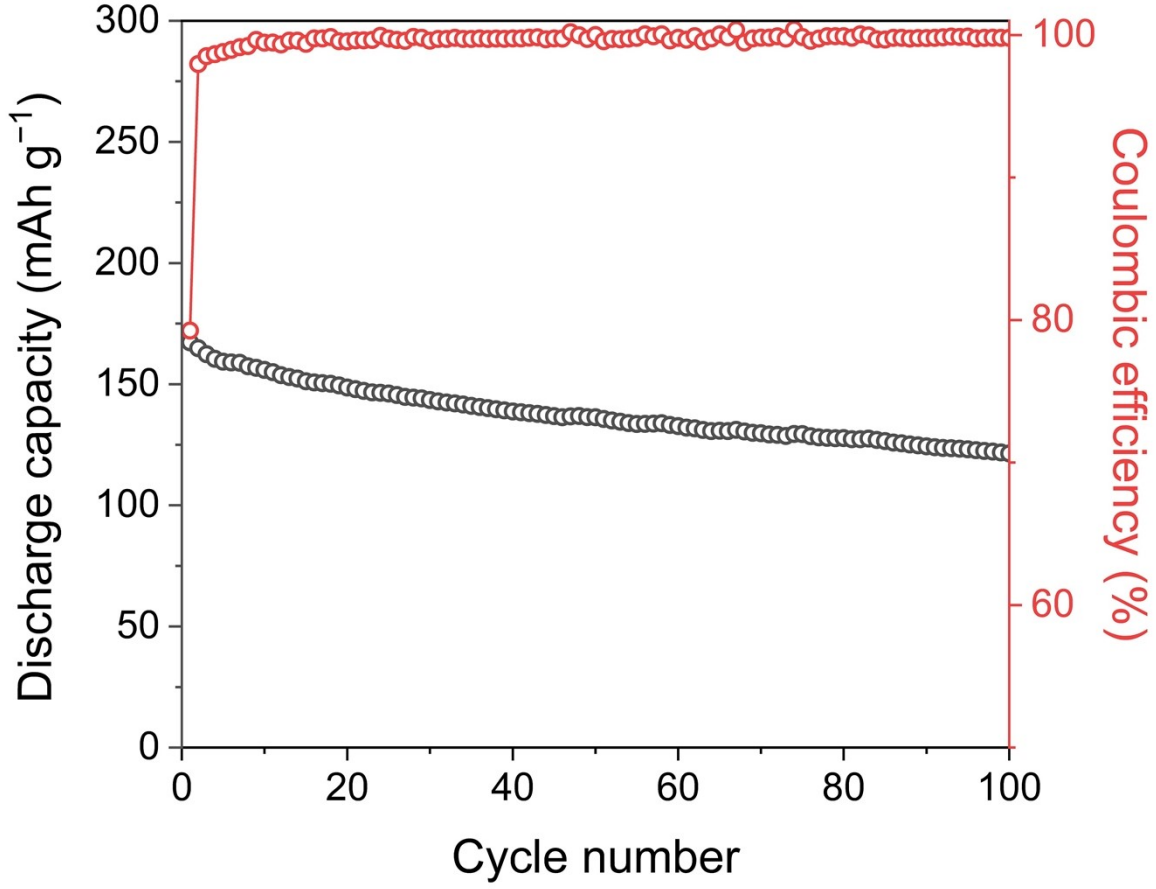

Fig. S14. Cycling performance at 0.5 C of the ASSB assembled with $Li_{5.35}PS_{4.35}(BH_4)_{1.15}Cl_{0.5}$ solid electrolyte (Cathode mixture/Solid electrolyte ($Li_{5.35}PS_{4.35}(BH_4)_{1.15}Cl_{0.5}$)/Li–In foil). The charge and discharge capacity were well maintained up to 100 cycles. The discharge capacity after 100 cycles at 0.5 C was 121.46 mAh g^{-1}, 72.6% of the initial discharge capacity.

Table S1. Ionic conductivity of Li_3PS_4+x$LiBH_4$.

$LiBH_4$ (mol)	Ionic conductivity (mS cm^{-1}) (at 25 °C, 188 MPa)
1	2.1
1.5	4.5
2	8.6
2.25	10.6
2.5	10.2
2.625	9.7

Table S2. Ionic conductivity of Li_3PS_4+x$LiBH_4$+yLiCl (x+y $\geq$ 2).

$LiBH_4$ (mol)	LiCl (mol)	Ionic conductivity (mS cm^{-1}) (at 25 °C, 188 MPa)
1	1	6.3
1.25	0.75	9.9
1.25	1	8.9
1.375	0.75	9.8
1.375	1	10.2
1.5	0.5	10.1
1.5	0.75	11.5
1.5	1	12.8
1.75	0.25	11.0
1.75	0.5	13.5
1.75	0.75	14.6
1.75	1	13.7
2	0.25	13.3
2	0.5	16.4
2	0.75	14.7
2	1	14.2
2.25	0.25	15.9
2.25	0.5	16.3
2.25	0.75	12.8
2.5	0.5	15.1

Table S3. Ionic conductivity of Li_3PS_4+x$LiBH_4$+yLiBr (x+y ≥ 2).

$LiBH_4$ (mol)	LiBr (mol)	Ionic conductivity (mS cm^{-1}) (at 25 °C, 188 MPa)
1.25	0.75	8.3
1.375	0.75	9.5
1.375	1	10.0
1.5	0.5	9.9
1.5	0.75	11.8
1.5	1	11.7
1.75	0.25	9.7
1.75	0.5	12.7
1.75	0.75	13.2
1.75	1	11.8
2	0.25	12.2
2	0.5	13.5
2	0.75	13.0
2	1	10.8
2.25	0.25	13.0
2.25	0.5	13.7
2.5	0.5	12.8

Table S4. Ionic conductivity of Li_3PS_4+x$LiBH_4$+yLiI (x+y ≥ 2).

$LiBH_4$ (mol)	LiI (mol)	Ionic conductivity (mS cm^{-1}) (at 25 °C, 188 MPa)
1.5	1	2.6
1.75	0.75	6.1
2	0.25	11.4
2	0.5	10.1

Table S5. Ionic conductivity of Li_3PS_4+x$LiBH_4$+yLiCl+zLiBr+kLiI (x+y+z+k ≥ 2).

$LiBH_4$ (mol)	LiCl (mol)	LiBr (mol)	LiI (mol)	Ionic conductivity (mS cm^{-1}) (at 25 °C, 188 MPa)
1	0.5	0.5	-	6.3
1	0.75	0.25	-	6.7
1	0.75	0.25	0.25	8.3
1.25	0.75	0.25	-	9.4
1.25	0.75	-	0.25	8.9
1.25	1	0.33	-	9.4
1.25	1	-	0.33	9.8
1.25	1	-	0.5	7.2
1.5	0.5	-	0.5	11.7
1.5	0.75	-	0.25	13.8
2	0.25	0.25	-	14.3
2	0.25	-	0.25	12.6
2	0.5	-	0.25	13.5
2	0.5	-	0.17	14.5

Table S6. Ionic radius of the halide anions, BH_4^- , and S^{2-} and volume per formula unit of lithium halide, lithium borohydride, and lithium sulfide.[9]

X^-	Ionic radius (Å)	LiX	Volume per formula unit ($Å^3$)
F^-	1.26	LiF	17.02
Cl^-	1.68	LiCl	32.86
Br^-	1.90	LiBr	40.37
I^-	2.11	LiI (Cubic)	53.15
BH_4^-	2.05	$LiBH_4$ (Orthorhombic)	49.91
S^{2-}	1.89	Li_2S	46.685

Table S7. Constraints employed for conducting Rietveld refinement on XRD data of the as-synthesized samples. The atomic positions of T5 were taken from Ref[10] and not refined in this study.

Atom	Site	x	y	z	Occupancy
Li	48h (T5)	0.3139	0.0219	0.6861	(7-Occ1-Occ2-0.5)/12
P	4b	0	0	0.5	1
S	16e	Pos1	−Pos1	0.5+Pos1	1
S	4d	0.25	0.25	0.75	0.75−Occ1
B	4d	0.25	0.25	0.75	Occ1
Cl	4d	0.25	0.25	0.75	0.25
S	4a	0	0	0	0.75−Occ2
B	4a	0	0	0	Occ2
Cl	4a	0	0	0	0.25
H	4d	0.31350	0.18650	0.81350	Occ1/2
H	4d	0.31350	0.31350	0.81350	Occ1/2
H	4a	0.06350	−0.06350	0.06350	Occ2/2
H	4a	0.06350	0.06350	0.06350	Occ2/2

Table S8. Rietveld refinement results of Li_3PS_4+1.5$LiBH_4$+0.5LiCl (T5 site from Table S7).

Atom	Site	x	y	z	Occupancy
Li	48h (T5)	0.3139	0.0219	0.6861	0.47(2)
P	4b	0	0	0.5	1
S	16e	0.1208(3)	−0.1208(3)	0.6208(3)	1
S	4d	0.25	0.25	0.75	0.290(16)
B	4d	0.25	0.25	0.75	0.460(16)
Cl	4d	0.25	0.25	0.75	0.25
S	4a	0	0	0	0.378(15)
B	4a	0	0	0	0.372(15)
Cl	4a	0	0	0	0.25
H	4d	0.31350	0.18650	0.81350	0.230(8)
H	4d	0.31350	0.31350	0.81350	0.230(8)
H	4a	0.06350	−0.06350	0.06350	0.187(7)
H	4a	0.06350	0.06350	0.06350	0.187(7)
Space group, F-43m; lattice parameter, a = 9.9497(9) Å; R_{wp} = 3.817%					

Table S9. Rietveld refinement results of Li_3PS_4+1.75$LiBH_4$+0.5LiCl (T5 site from Table S7).

Atom	Site	x	y	z	Occupancy
Li	48h (T5)	0.3139	0.0219	0.6861	0.455(18)
P	4b	0	0	0.5	1
S	16e	0.1189(2)	−0.1189(2)	0.6189(2)	1
S	4d	0.25	0.25	0.75	0.257(12)
B	4d	0.25	0.25	0.75	0.493(12)
Cl	4d	0.25	0.25	0.75	0.25
S	4a	0	0	0	0.202(12)
B	4a	0	0	0	0.548(12)
Cl	4a	0	0	0	0.25
H	4d	0.31350	0.18650	0.81350	0.247(6)
H	4d	0.31350	0.31350	0.81350	0.247(6)
H	4a	0.06350	−0.06350	0.06350	0.274(6)
H	4a	0.06350	0.06350	0.06350	0.274(6)
Space group, F-43m; lattice parameter, a = 9.9587(8) Å; R_{wp} = 3.509%					

Table S10. Rietveld refinement results of Li_3PS_4+2.25$LiBH_4$+0.5LiCl (T5 site from Table S7).

Atom	Site	x	y	z	Occupancy
Li	48h (T5)	0.3139	0.0219	0.6861	0.437(19)
P	4b	0	0	0.5	1
S	16e	0.1190(3)	−0.1190(3)	0.6190(3)	1
S	4d	0.25	0.25	0.75	0.225(13)
B	4d	0.25	0.25	0.75	0.525(13)
Cl	4d	0.25	0.25	0.75	0.25
S	4a	0	0	0	0.021(13)
B	4a	0	0	0	0.729(13)
Cl	4a	0	0	0	0.25
H	4d	0.31350	0.18650	0.81350	0.262(6)
H	4d	0.31350	0.31350	0.81350	0.262(6)
H	4a	0.06350	−0.06350	0.06350	0.365(7)
H	4a	0.06350	0.06350	0.06350	0.365(7)
Space group, F-43m; lattice parameter, a = 9.9696(7) Å; R_{wp} = 3.845%					

Table S11. Rietveld refinement results of Li_3PS_4+2.5$LiBH_4$+0.5LiCl (T5 site from Table S7).

Atom	Site	x	y	z	Occupancy
Li	48h (T5)	0.3139	0.0219	0.6861	0.43(3)
P	4b	0	0	0.5	1
S	16e	0.1185(3)	−0.1185(3)	0.6185(3)	1
S	4d	0.25	0.25	0.75	0.206(19)
B	4d	0.25	0.25	0.75	0.544(19)
Cl	4d	0.25	0.25	0.75	0.25
S	4a	0	0	0	0.000(17)
B	4a	0	0	0	0.750(17)
Cl	4a	0	0	0	0.25
H	4d	0.31350	0.18650	0.81350	0.272(9)
H	4d	0.31350	0.31350	0.81350	0.272(9)
H	4a	0.06350	−0.06350	0.06350	0.373(8)
H	4a	0.06350	0.06350	0.06350	0.373(8)
Space group, F-43m; lattice parameter, a = 9.9714(10) Å; R_{wp} = 4.022%					

Table S12. Constraints employed for conducting Rietveld refinement on XRD data of the as-synthesized samples with T5 site different from that in Table S7. The atomic positions of T5 were taken from Ref[11] and not refined in this study (ICSD collection code #142464).

Atom	Site	x	y	z	Occupancy
Li	48h (T5)	0.3055	0.0231	0.6945	(7-Occ1-Occ2-0.5)/12
P	4b	0	0	0.5	1
S	16e	Pos1	−Pos1	0.5+Pos1	1
S	4d	0.25	0.25	0.75	0.75−Occ1
B	4d	0.25	0.25	0.75	Occ1
Cl	4d	0.25	0.25	0.75	0.25
S	4a	0	0	0	0.75−Occ2
B	4a	0	0	0	Occ2
Cl	4a	0	0	0	0.25
H	4d	0.31350	0.18650	0.81350	Occ1/2
H	4d	0.31350	0.31350	0.81350	Occ1/2
H	4a	0.06350	−0.06350	0.06350	Occ2/2
H	4a	0.06350	0.06350	0.06350	Occ2/2

Table S13. Rietveld refinement results of Li_3PS_4+1.5$LiBH_4$+0.5LiCl (T5 site from Table S12).

Atom	Site	x	y	z	Occupancy
Li	48h (T5)	0.3055	0.0231	0.6945	0.47(4)
P	4b	0	0	0.5	1
S	16e	0.1202(3)	−0.1202(3)	0.6202(3)	1
S	4d	0.25	0.25	0.75	0.24(2)
B	4d	0.25	0.25	0.75	0.51(2)
Cl	4d	0.25	0.25	0.75	0.25
S	4a	0	0	0	0.46(3)
B	4a	0	0	0	0.29(3)
Cl	4a	0	0	0	0.25
H	4d	0.31350	0.18650	0.81350	0.253(11)
H	4d	0.31350	0.31350	0.81350	0.253(11)
H	4a	0.06350	−0.06350	0.06350	0.147(14)
H	4a	0.06350	0.06350	0.06350	0.147(14)
Space group, F-43m; lattice parameter, a = 9.9506(10) Å; R_{wp} = 4.132%					

Table S14. Rietveld refinement results of Li_3PS_4+1.75$LiBH_4$+0.5LiCl (T5 site from Table S12).

Atom	Site	x	y	z	Occupancy
Li	48h (T5)	0.3055	0.0231	0.6945	0.45(3)
P	4b	0	0	0.5	1
S	16e	0.1182(2)	−0.1182(2)	0.6182(2)	1
S	4d	0.25	0.25	0.75	0.20(2)
B	4d	0.25	0.25	0.75	0.55(2)
Cl	4d	0.25	0.25	0.75	0.25
S	4a	0	0	0	0.26(2)
B	4a	0	0	0	0.49(2)
Cl	4a	0	0	0	0.25
H	4d	0.31350	0.18650	0.81350	0.274(10)
H	4d	0.31350	0.31350	0.81350	0.274(10)
H	4a	0.06350	−0.06350	0.06350	0.245(12)
H	4a	0.06350	0.06350	0.06350	0.245(12)
Space group, F-43m; lattice parameter, a = 9.9595(9) Å; R_{wp} = 3.83%					

Table S15. Rietveld refinement results of Li_3PS_4+2$LiBH_4$+0.5LiCl (T5 site from Table S12).

Atom	Site	x	y	z	Occupancy
Li	48h (T5)	0.3055	0.0231	0.6945	0.44(3)
P	4b	0	0	0.5	1
S	16e	0.1183(3)	−0.1183(3)	0.6183(3)	1
S	4d	0.25	0.25	0.75	0.16(2)
B	4d	0.25	0.25	0.75	0.59(2)
Cl	4d	0.25	0.25	0.75	0.25
S	4a	0	0	0	0.20(2)
B	4a	0	0	0	0.55(2)
Cl	4a	0	0	0	0.25
H	4d	0.31350	0.18650	0.81350	0.295(10)
H	4d	0.31350	0.31350	0.81350	0.295(10)
H	4a	0.06350	−0.06350	0.06350	0.274(12)
H	4a	0.06350	0.06350	0.06350	0.274(12)
Space group, F-43m; lattice parameter, a = 9.9671(8) Å; R_{wp} = 4.099%					

Table S16. Rietveld refinement results of Li_3PS_4+2.25$LiBH_4$+0.5LiCl (T5 site from Table S12).

Atom	Site	x	y	z	Occupancy
Li	48h (T5)	0.3055	0.0231	0.6945	0.44(3)
P	4b	0	0	0.5	1
S	16e	0.1183(3)	−0.1183(3)	0.6183(3)	1
S	4d	0.25	0.25	0.75	0.16(2)
B	4d	0.25	0.25	0.75	0.59(2)
Cl	4d	0.25	0.25	0.75	0.25
S	4a	0	0	0	0.09(2)
B	4a	0	0	0	0.66(2)
Cl	4a	0	0	0	0.25
H	4d	0.31350	0.18650	0.81350	0.293(10)
H	4d	0.31350	0.31350	0.81350	0.293(10)
H	4a	0.06350	−0.06350	0.06350	0.331(12)
H	4a	0.06350	0.06350	0.06350	0.331(12)
Space group, F-43m; lattice parameter, a = 9.9699(8) Å; R_{wp} = 4.137%					

Table S17. Rietveld refinement results of Li_3PS_4+2.5$LiBH_4$+0.5LiCl (T5 site from Table S12).

Atom	Site	x	y	z	Occupancy
Li	48h (T5)	0.3055	0.0231	0.6945	0.43(2)
P	4b	0	0	0.5	1
S	16e	0.1183(3)	−0.1183(3)	0.6183(3)	1
S	4d	0.25	0.25	0.75	0.15(2)
B	4d	0.25	0.25	0.75	0.60(2)
Cl	4d	0.25	0.25	0.75	0.25
S	4a	0	0	0	0.06(2)
B	4a	0	0	0	0.69(2)
Cl	4a	0	0	0	0.25
H	4d	0.31350	0.18650	0.81350	0.302(10)
H	4d	0.31350	0.31350	0.81350	0.302(10)
H	4a	0.06350	−0.06350	0.06350	0.344(12)
H	4a	0.06350	0.06350	0.06350	0.344(12)
Space group, F-43m; lattice parameter, a = 9.9774(8) Å; R_{wp} = 4.319%					

Table S18. Rietveld refinement results of Li_3PS_4+2$LiBH_4$ (T5 site from Table S7).

Atom	Site	x	y	z	Occupancy
Li	48h (T5)	0.3139	0.0219	0.6861	0.47(4)
P	4b	0	0	0.5	1
S	16e	0.1211(6)	−0.1211(6)	0.6211(6)	1
S	4d	0.25	0.25	0.75	0.38(3)
B	4d	0.25	0.25	0.75	0.62(3)
S	4a	0	0	0	0.21(3)
B	4a	0	0	0	0.79(3)
H	4d	0.31350	0.18650	0.81350	0.311(14)
H	4d	0.31350	0.31350	0.81350	0.311(14)
H	4a	0.06350	−0.06350	0.06350	0.393(13)
H	4a	0.06350	0.06350	0.06350	0.393(13)
Space group, F-43m; lattice parameter, a = 10.009(2) Å; R_{wp} = 4.737%					

Table S19. Comparison of the room-temperature ionic conductivity (σ) between this study and literature for argyrodites with 1.5 or more halide substitutions and superionic argyrodites.

Materials	σ (mS cm^{-1})	Measurement Condition	Reference
$Li_{5.35}PS_{4.35}(BH_4)_{1.15}Cl_{0.5}$	16.4	Cold-pressed	This study
$Li_{5.35}PS_{4.35}(BH_4)_{1.15}Cl_{0.5}$	26.1	Sintered	This study
$Li_{5.5}PS_{4.5}Cl_{1.5}$	9.4	Cold-pressed	12
	12	Sintered	
	9.03	Cold-pressed	13
	7.2	Cold-pressed	4
	10.2	Cold-pressed	7
	8.3	Cold-pressed	14
$Li_{5.3}PS_{4.3}Cl_{1.7}$	7.0	Cold-pressed	
	17	Sintered	15
$Li_{5.3}PS_{4.3}ClBr_{0.7}$	24	Sintered	6
$Li_{5.5}PS_{4.5}ClBr_{0.5}$	17	Sintered	
$Li_{5.2}Si_{0.2}Sb_{0.8}S_4Br_{0.25}I_{1.75}$	13.23	Cold-pressed	16
$Li_{6.6}Si_{0.6}Sb_{0.4}S_5I$	14.8	Cold-pressed	17
$Li_{6.6}Si_{0.6}Sb_{0.4}S_5I$	24	Sintered	
$Li_{6.5}Sb_{0.5}Ge_{0.5}S_5I$	16.1	Cold-pressed	18
$Li_{6.75}Sb_{0.25}Si_{0.75}S_5I$	13.1	Cold-pressed	19

Table S20. Constraints employed for conducting Rietveld refinement on XRD data of the annealed samples (identical Cl^- occupancies at 4a and 4d sites, T5 site from Table S7).

Atom	Site	x	y	z	Occupancy
Li	48h (T5)	0.3139	0.0219	0.6861	(7-Occ1-Occ2-0.5)/12
P	4b	0	0	0.5	1
S	16e	Pos1	−Pos1	0.5+Pos1	1
S	4d	0.25	0.25	0.75	0.75−Occ1
B	4d	0.25	0.25	0.75	Occ1
Cl	4d	0.25	0.25	0.75	0.25
S	4a	0	0	0	0.75−Occ2
B	4a	0	0	0	Occ2
Cl	4a	0	0	0	0.25
H	4d	0.31350	0.18650	0.81350	Occ1/2
H	4d	0.31350	0.31350	0.81350	Occ1/2
H	4a	0.06350	−0.06350	0.06350	Occ2/2
H	4a	0.06350	0.06350	0.06350	Occ2/2

Table S21. Rietveld refinement results of Li_3PS_4+2$LiBH_4$+0.5LiCl annealed at 300 °C (identical Cl^- occupancies at 4a and 4d sites, T5 site from Table S7).

Atom	Site	x	y	z	Occupancy
Li	48h (T5)	0.3139	0.0219	0.6861	0.50(2)
P	4b	0	0	0.5	1
S	16e	0.1218(3)	−0.1218(3)	0.6218(3)	1
S	4d	0.25	0.25	0.75	0.750(16)
B	4d	0.25	0.25	0.75	0.000(16)
Cl	4d	0.25	0.25	0.75	0.25
S	4a	0	0	0	0.750(14)
B	4a	0	0	0	0.000(14)
Cl	4a	0	0	0	0.25
H	4d	0.31350	0.18650	0.81350	0.000(8)
H	4d	0.31350	0.31350	0.81350	0.000(8)
H	4a	0.06350	−0.06350	0.06350	0.000(7)
H	4a	0.06350	0.06350	0.06350	0.000(7)
Space group, F-43m; lattice parameter, a = 9.9109(8) Å; R_{wp} = 3.314%					

Table S22. Constraints employed for conducting Rietveld refinement on XRD data of the annealed samples (no restriction on the Cl^- occupancies at 4a and 4d sites, T5 site from Table S7).

Atom	Site	x	y	z	Occupancy
Li	48h (T5)	0.3139	0.0219	0.6861	(7-Occ1-Occ3-0.5)/12
P	4b	0	0	0.5	1
S	16e	Pos1	−Pos1	0.5+Pos1	1
S	4d	0.25	0.25	0.75	1−Occ1−Occ2
B	4d	0.25	0.25	0.75	Occ1
Cl	4d	0.25	0.25	0.75	Occ2
S	4a	0	0	0	0.5−Occ3+Occ2
B	4a	0	0	0	Occ3
Cl	4a	0	0	0	0.5−Occ2
H	4d	0.31350	0.18650	0.81350	Occ1/2
H	4d	0.31350	0.31350	0.81350	Occ1/2
H	4a	0.06350	−0.06350	0.06350	Occ3/2
H	4a	0.06350	0.06350	0.06350	Occ3/2

Table S23. Rietveld refinement results of Li_3PS_4+2.5$LiBH_4$+0.5LiCl annealed at 300 °C (no restriction on the Cl^- occupancies at 4a and 4d sites, T5 site from Table S7).

Atom	Site	x	y	z	Occupancy
Li	48h (T5)	0.3139	0.0219	0.6861	0.510(19)
P	4b	0	0	0.5	1
S	16e	0.1218(3)	−0.1218(3)	0.6218(3)	1
S	4d	0.25	0.25	0.75	0.55(19)
B	4d	0.25	0.25	0.75	0.00(4)
Cl	4d	0.25	0.25	0.75	0.45(19)
S	4a	0	0	0	0.9(2)
B	4a	0	0	0	0.00(4)
Cl	4a	0	0	0	0.05(19)
H	4d	0.31350	0.18650	0.81350	0.000(18)
H	4d	0.31350	0.31350	0.81350	0.000(18)
H	4a	0.06350	−0.06350	0.06350	0.00(2)
H	4a	0.06350	0.06350	0.06350	0.00(2)
Space group, F-43m; lattice parameter, a = 9.9121(7) Å; R_{wp} = 3.469%					

Table S24. Comparison of the critical current density (CCD) between this study and literature for argyrodites. The 'CP', 'ST', 'PL', and 'PD' abbreviations are 'cold-pressed', 'sintered', 'pellet', and 'powder', respectively. The 'TC', and 'CC' abbreviations are 'time-constant mode measurement', and 'capacity-constant mode measurement', respectively. A dash indicates that the value was not reported.

Materials	CCD (mA cm^{-2})	Cell Fabrication Condition	Measurement Condition	Stack Pressure	Reference
$Li_{5.35}PS_{4.35}(BH_4)_{1.15}Cl_{0.5}$	2.1	PD, CP	TC, 30 °C	7 N m (Torque)	This study
$Li_{5.35}PS_{4.35}(BH_4)_{1.15}Cl_{0.5}$	2.5	PD, CP	CC, 30 °C	7 N m (Torque)	This study
Li_6PS_5Cl	1.05	PL, ST	TC, 25 °C	-	20
	0.55	PD, ST		-	
LPS-LiI	0.35–1	PD, CP	TC, 25 °C	-	21
Li_6PS_5Cl	0.2	PD, CP	TC, 25 °C	-	22
Li_6PS_5Cl-MoO_2	0.55	PD, CP	TC, 25 °C	-	
Li_6PS_5Cl	0.53	PD, CP	TC, 25 °C	-	23
Li_6PS_5Cl	0.2	PD, CP	TC	-	24
Li_6PS_5Cl	2.4	PD, CP	CC, 28 °C	19 MPa	25
Li_6PS_5Cl	0.95	PD, CP	TC, 25 °C	-	26
$Li_{5.5}PS_{4.5}Cl_{1.5}$	1.40	PD, CP	TC, 25 °C	-	
	1.08	PD, CP	TC, 25 °C	-	
Li_6PS_5Cl	1.0	PL, ST	CC, 30 °C	4.6 MPa	27
Li_6PS_5Br	0.45	PD, CP	TC, 30 °C	-	28
$Li_{5.5}P_{0.96}Sb_{0.04}S_{4.4}O_{0.1}Cl_{1.5}$	1.5	PD, CP	TC, 25 °C	-	29
$Li_{6.4}PS_{5.4}Cl_{0.6}$	0.70	PD, CP	TC, 24 ± 4 °C	-	30
Li_6PS_5Cl	0.95				
$Li_{5.7}PS_{4.7}Cl_{1.3}$	1.05				
$Li_{5.3}PS_{4.3}Cl_{1.6}$	0.56				

References

1 D. A. Ziolkowska, W. Arnold, T. Druffel, M. Sunkara and H. Wang, *ACS Appl Mater Interfaces*, 2019, **11**, 6015-6021.
2 A. A. Coelho, *Journal of Applied Crystallography*, 2018, **51**, 210-218.
3 Y. Filinchuk, D. Chernyshov and V. Dmitriev, *Zeitschrift für Kristallographie*, 2008, **223**, 649-659.
4 A. Gautam, M. Ghidiu, E. Suard, M. A. Kraft and W. G. Zeier, *ACS Applied Energy Materials*, 2021, **4**, 7309-7315.
5 Y. Liu, H. Peng, H. Su, Y. Zhong, X. Wang, X. Xia, C. Gu and J. Tu, *Adv Mater*, 2022, **34**, e2107346.
6 S. V. Patel, S. Banerjee, H. Liu, P. Wang, P.-H. Chien, X. Feng, J. Liu, S. P. Ong and Y.-Y. Hu, *Chemistry of Materials*, 2021, **33**, 1435-1443.
7 W. D. Jung, J. S. Kim, S. Choi, S. Kim, M. Jeon, H. G. Jung, K. Y. Chung, J. H. Lee, B. K. Kim, J. H. Lee and H. Kim, *Nano Lett*, 2020, **20**, 2303-2309.
8 K. Momma and F. Izumi, *Journal of Applied Crystallography*, 2011, **44**, 1272-1276.
9 M. C. Simoes, K. J. Hughes, D. B. Ingham, L. Ma and M. Pourkashanian, *Inorg Chem*, 2017, **56**, 7566-7573.
10 A. Gautam, M. Sadowski, M. Ghidiu, N. Minafra, A. Senyshyn, K. Albe and W. G. Zeier, *Advanced Energy Materials*, 2020, **11**.
11 N. Minafra, M. A. Kraft, T. Bernges, C. Li, R. Schlem, B. J. Morgan and W. G. Zeier, *Inorg Chem*, 2020, **59**, 11009-11019.
12 P. Adeli, J. D. Bazak, K. H. Park, I. Kochetkov, A. Huq, G. R. Goward and L. F. Nazar, *Angew Chem Int Ed Engl*, 2019, **58**, 8681-8686.
13 L. Peng, C. Yu, Z. Zhang, H. Ren, J. Zhang, Z. He, M. Yu, L. Zhang, S. Cheng and J. Xie, *Chemical Engineering Journal*, 2022, **430**.
14 S. Wang, A. Gautam, X. Wu, S. Li, X. Zhang, H. He, Y. Lin, Y. Shen and C.-W. Nan, *Advanced Energy and Sustainability Research*, 2023, DOI: 10.1002/aesr.202200197.
15 X. Feng, P.-H. Chien, Y. Wang, S. Patel, P. Wang, H. Liu, M. Immediato-Scuotto and Y.-Y. Hu, *Energy Storage Materials*, 2020, **30**, 67-73.
16 W. D. Jung, J. S. Kim, Y. J. Kim, H. Jeong, D. Han, K. W. Nam, D. Ahn, D. H. Kwon, H. G. Jung, J. H. Lee and H. Kim, *Advanced Functional Materials*, 2022, DOI: 10.1002/adfm.202211185.
17 L. Zhou, A. Assoud, Q. Zhang, X. Wu and L. F. Nazar, *J Am Chem Soc*, 2019, **141**, 19002-19013.
18 Y. Lee, J. Jeong, H. J. Lee, M. Kim, D. Han, H. Kim, J. M. Yuk, K.-W. Nam, K. Y. Chung, H.-G. Jung and S. Yu, *ACS Energy Letters*, 2021, **7**, 171-179.
19 Y. Lee, J. Jeong, H.-D. Lim, S.-O. Kim, H.-G. Jung, K. Y. Chung and S. Yu, *ACS Sustainable Chemistry & Engineering*, 2020, **9**, 120-128.
20 G. Liu, W. Weng, Z. Zhang, L. Wu, J. Yang and X. Yao, *Nano Lett*, 2020, **20**, 6660-6665.
21 F. Han, J. Yue, X. Zhu and C. Wang, *Advanced Energy Materials*, 2018, **8**.
22 Y. Subramanian, R. Rajagopal, S. Kang and K.-S. Ryu, *Journal of Alloys and Compounds*, 2022, **925**.
23 Z. Zhang, L. Zhang, Y. Liu, X. Yan, B. Xu and L.-m. Wang, *Journal of Alloys and Compounds*, 2020, **812**.
24 Y. Subramanian, R. Rajagopal and K.-S. Ryu, *Journal of Alloys and Compounds*, 2023, **940**.
25 J. A. Lewis, C. Lee, Y. Liu, S. Y. Han, D. Prakash, E. J. Klein, H. W. Lee and M. T. McDowell, *ACS Appl Mater Interfaces*, 2022, **14**, 4051-4060.
26 Y. Liu, H. Su, Y. Zhong, X. Wang, X. Xia, C. Gu and J. Tu, *Advanced Functional Materials*, 2022, **32**.
27 J. Su, M. Pasta, Z. Ning, X. Gao, P. G. Bruce and C. R. M. Grovenor, *Energy & Environmental Science*, 2022, **15**, 3805-3814.
28 Z. Zhang, L. Zhang, X. Yan, H. Wang, Y. Liu, C. Yu, X. Cao, L. van Eijck and B. Wen, *Journal of Power Sources*, 2019, **410-411**, 162-170.
29 C. Wei, C. Yu, R. Wang, L. Peng, S. Chen, X. Miao, S. Cheng and J. Xie, *Journal of Power Sources*, 2023, **559**.
30 D. Zeng, J. Yao, L. Zhang, R. Xu, S. Wang, X. Yan, C. Yu and L. Wang, *Nat Commun*, 2022, **13**, 1909.